



HAL
open science

Semi-automatic extraction of functional dynamic networks describing patient's epileptic seizures

Gaëtan Frusque, Pierre Borgnat, Paulo Gonçalves, Julien Jung

► To cite this version:

Gaëtan Frusque, Pierre Borgnat, Paulo Gonçalves, Julien Jung. Semi-automatic extraction of functional dynamic networks describing patient's epileptic seizures. *Frontiers in Neurology*, In press, pp.1-24. 10.3389/fneur.2020.579725 . hal-02935666v1

HAL Id: hal-02935666

<https://inria.hal.science/hal-02935666v1>

Submitted on 10 Sep 2020 (v1), last revised 7 Jan 2021 (v2)

HAL is a multi-disciplinary open access archive for the deposit and dissemination of scientific research documents, whether they are published or not. The documents may come from teaching and research institutions in France or abroad, or from public or private research centers.

L'archive ouverte pluridisciplinaire **HAL**, est destinée au dépôt et à la diffusion de documents scientifiques de niveau recherche, publiés ou non, émanant des établissements d'enseignement et de recherche français ou étrangers, des laboratoires publics ou privés.

Semi-automatic extraction of functional dynamic networks describing patient's epileptic seizures

Gaëtan Frusque^{1,*}, Pierre Borgnat², Paulo Gonçalves¹ and Julien Jung^{3,4}

¹Univ Lyon, Inria, CNRS, ENS de Lyon, UCB Lyon 1, LIP UMR 5668, F-69342, Lyon, France

²Univ Lyon, CNRS, ENS de Lyon, UCB Lyon 1, Laboratoire de Physique, UMR 5672, F-69342 Lyon, France

³National Institute of Health and Medical Research U1028/National Center for Scientific Research, Mixed Unit of Research 5292, Lyon Neuroscience Research Center, Lyon, France.

⁴Department of Functional Neurology and Epileptology, Member of the ERN EpiCARE Lyon University Hospital and Lyon 1 University, Lyon, France.

Correspondence*:

Gaëtan Frusque

gaetan.frusque@ens-lyon.fr

2 ABSTRACT

3 Intracranial EEG studies using stereotactic EEG (SEEG) have shown that during seizures,
4 epileptic activity spreads across several anatomical regions from the seizure onset zone towards
5 remote brain areas. A full and objective characterisation of this patient-specific time-varying
6 network is crucial for optimal surgical treatment. Functional Connectivity (FC) analysis of SEEG
7 signals recorded during seizures enables to describe the statistical relations between all pairs
8 of recorded signals. However, extracting meaningful information from those large datasets is
9 time-consuming and requires high expertise.

10 In the present study, we first propose a novel method named Brain-wide Time-varying Network
11 Decomposition (BTND) to characterise the dynamic epileptogenic networks activated during
12 seizures in individual patients recorded with SEEG electrodes. The method provides a number of
13 pathological FC subgraphs with their temporal course of activation. The method can be applied
14 to several seizures of the patient to extract reproducible subgraphs. Secondly, we compare the
15 activated subgraphs obtained by the BTND method with visual interpretation of SEEG signals
16 recorded in 27 seizures from 9 different patients. As a whole, we found that activated subgraphs
17 corresponded to brain regions involved during the course of the seizures and their time course
18 were highly consistent with classical visual interpretation. We believe that the proposed method
19 can complement the visual analysis of SEEG signals recorded during seizures by highlighting
20 and characterising the most significant parts of epileptic networks with their activation dynamics.

21 **Keywords:** epilepsy, functional connectivity, SEEG, epileptogenic networks, dynamical graph, subgraphs extraction

1 INTRODUCTION

22 About 30 to 40% of epileptic patients are drug-resistant [42]. For those patients, surgical resection of the
23 epileptogenic brain structures is considered to promote seizure freedom [42]. Intracranial EEG using depth
24 EEG recordings or the stereoecephalography (SEEG) method is often required to guide tailored-surgical
25 resection. [18, 22].

26 The primary aim of SEEG is to delineate precisely the epileptogenic regions. However, since the
27 pioneering works in SEEG, it has been shown that seizures can not be considered as static phenomena with
28 a single focus activation leading to clinical manifestations [13]. SEEG recordings of focal seizures typically
29 show that the epileptic activity spreads during seizures across several anatomical regions. It begins at the
30 seizure onset zone and spreads towards remote brain areas. This dynamical pathological process can be
31 described by several brain states characterised by transient and abnormal connectivity profiles within the
32 epileptogenic network [7]. A full and objective characterisation of this patient-specific dynamic network is
33 crucial for optimal surgical treatment.

34 Understanding brain network modifications operating at different time scales in the interictal state and
35 during seizures is a very active stream of research. This is in line with computational neuroscience studies
36 modelling neurological diseases as brain network disease ([19], [48], [46], [41], [43], [1]).

37 In the field of epileptology, the structure of epileptic (or ictal) networks has been explored using
38 connectivity analysis (functional or effective connectivity) and more recently, graph-theory analysis [7].
39 Functional connectivity (FC) approaches, based on linear or non-linear measures, quantify the statistical
40 relations between any pair of recorded SEEG signals and their evolution across time. In most of the studies,
41 pairwise correlations between remote sites are computed at specific time points (for a review, see [7]).
42 Those approaches unveil the organisational interactions of different regions of interest in the brains. They
43 have proved very fruitful to investigate the neurophysiological correlations of symptoms during seizures,
44 or to describe several subtypes of focal epilepsy involving specific networks [8], [6], [4]. Graph theory is
45 the study of graphs, which are mathematical structures used to model networks, and specifically pairwise
46 relations between objects [44], [46]. A graph is made of vertices (also called nodes) which are connected
47 by edges. Graph theory approaches allow the description of both local and global characteristics [10]. For
48 epilepsy, the nodes usually represent electrode contacts and the edges represent the (FC) measures. The
49 resulting graph structure is known to contain relevant fingerprints of the seizure dynamic. Studying network
50 structures with graph theory provides mathematical tools to investigate different subtypes of epilepsy [21].
51 For example, it has been shown that the properties of networks' topology are different for temporal lobe,
52 mesial temporal lobe and neocortical epilepsy [3]. Moreover, some studies suggest that investigating local
53 properties of the network structure through graph theory concepts provides biomarkers for epileptogenic
54 focus localisation [47], [51] [53]. Lastly, dynamic graph theory can also provide step-by-step modelling of
55 the propagation of the seizure in the brain [47], [11].

56 A major challenge for the study of ictal networks is that seizures are a highly dynamical process with
57 rapid transitions between network states [29], [7]. To track network changes during the seizures, the
58 network organisation has to be described at short time scales. In the most straightforward approach, FC
59 forming the backbone of the network are estimated at different time steps of the seizure. Therefore, they are
60 prone to create spurious connections and constitute a noisy estimation of the pathologic dynamic network.
61 Moreover, as the brain activity is commonly monitored with more than one hundred electrode contacts
62 distributed along the stereotactic rods, the number of FC scales quadratically (100 electrode contacts
63 providing around 5000 FC measures), making the study of FC over time a resources consuming task that
64 requires high expertise.

65 One advantage of SEEG monitoring is to allow the recording of several seizures from the same patient,
 66 with the same measurement points (or nodes), yielding thus as many realisations of identically distributed
 67 dynamical networks of FC. Hence, several seizures from the same patient can be investigated, that may
 68 share some connectivity features but with different dynamics. Methodological tools have to be proposed
 69 to extract relevant information from those large datasets. Ideally, such methods should summarise the
 70 dynamics of the seizures by providing several epileptogenic networks, with stable network structures, that
 71 characterise the different steps of the seizures and that are involved in the production and the propagation
 72 of the ictal events. Those network states may be common to the different seizures of the patient, but the
 73 timeline activation should follow a pattern that remains specific to each seizure [11].

74 Along these lines, we propose a novel semi-automatic method to characterise the dynamic epileptogenic
 75 network quantitatively and across time using SEEG signals. We propose to perform the joint analysis
 76 of all seizures of the same patient, firstly to reduce the measurement uncertainty in the calculation of
 77 FC indices, and secondly, to make robust the identification of a time-functional pattern, systematic in all
 78 seizures and characteristic of a patient's pathology. First, the full FC matrix is computed for each time
 79 step using a classical FC measure, namely the Phase Locking Value [33], [2]. Then, the method extracts
 80 several pathological subgraphs with their own activation score during seizures. We expect each subgraph
 81 to comprise several brain nodes with high connectivity values. The paper is organised as follows: We
 82 extend our previous work [17] to seizures with different durations, we call this method the Brain-wide
 83 Time-varying Network Decomposition (BTND). On the application side, we validate the clinical use of the
 84 method on a larger clinical dataset.

2 MATERIAL AND METHODS

85 2.1 Description of the Brain-wide Time-varying Network Decomposition (BTND 86 method)

87 For each patient, the dataset is composed of several SEEG recordings for different seizures. Seizures
 88 can have different durations. The proposed strategy can be summarised in four steps: (a) We chop each
 89 recording into short segments, (b) For each segment, we estimate via FC measures, the connectivity for
 90 each pair of electrode contacts. (c) We rearrange the FC measures into a list of matrices representing
 91 the time evolution of FC for each seizure of a patient. (d) The list of matrices representing the multi-
 92 seizures brain-wide time-varying network is decomposed into FC subgraphs characteristic of one patient
 93 but common to all his seizures, along with their activation profile specific to each seizure. The main steps
 94 of the method are illustrated in figure 1.

95 2.2 Representation of the multi-seizure brain-wide time-varying network

96 Practically, FC measurements are stored in a three-dimensional structure $\mathbf{X}_{lt}\{s\}$ corresponding to the FC
 97 of index l at time segment t and for the seizure s . The list of matrix $\mathbf{X}\{s\} \in \mathbb{R}^{L \times T(s)} \forall s (1, \dots, S)$ is the
 98 mathematical representation of the multi-seizures brain-wide time-varying network. Here S is the total
 99 number of seizures recorded for the same patient. We remind that the number of time steps $T(s)$ can vary
 100 for each seizure. Fig. 1.(c) illustrates an example of list of matrices $\mathbf{X}\{s\}$.

101 2.3 The optimization problem related to the BTND method

The core of the BTND method is then to seek, for each seizure, for the following decomposition:

$$\mathbf{X}\{s\} \approx \mathbf{F}\mathbf{V}^t\{s\} \quad (1)$$

102 where $\mathbf{F} \in \mathbb{R}^{L \times K}$ contains the K FC subgraphs and $\mathbf{V}\{s\} \in \mathbb{R}^{T(s) \times K}$ are their respective temporal
 103 activations corresponding to the specific seizure s . This approach directly entails the requested

104 decomposition since the columns of the matrix \mathbf{F} contains the weights of the edges in the sub-graphs, as it
 105 can be seen on figure 1.(d) and matrices $\mathbf{V}\{s\}$ directly correspond to the activation profiles of each seizure
 106 depicted figure 1.(d).

107 However, the solution for the decomposition (1) is not unique, and to favour handily interpretability from
 108 the medical viewpoint, we impose several constraints on the components \mathbf{F} and $\mathbf{V}\{s\}$:

- 109 a) Because most of the functional connectivity measures and activation indices are naturally positive
 110 values, we impose \mathbf{F} and \mathbf{V} to be **non-negative** matrices;
- 111 b) To limit the complexity of the inferred subgraphs, we restrict the number of non-zero significant FC
 112 values, yielding a sparse matrix \mathbf{F} . The **sparsity** constraint is meaningful in the context of epilepsy,
 113 where a large number of functional connectivities can be passively implied in the neurological process.
- c) To promote FC subgraphs that are continuously activate over specific periods, we impose **sparsity** and
compactness on $\mathbf{V}\{s\}$. These two constraints drastically improve the interpretability of the solution, as
 they prompt sparse and piecewise continuous activation periods that are close to cluster-like solutions.
 Formally, they correspond to the fused lasso constraint that reads:

$$C(\mathbf{v}, \gamma, \eta) : \gamma \sum_{t=1}^T |v_t| + \eta \sum_{t=1}^{T-1} |v_{t+1} - v_t| + \sum_{t=1}^T v_t^2 \leq 1, \quad (2)$$

114 where the parameter γ and the parameter η compel each activation profile $\mathbf{v} = \mathbf{V}_{:k}\{s\}$, to be sparse
 115 and compact, respectively. As for the third term in expression (2), it prevents incoherent solutions due
 116 to scaling indeterminacy [38].

Finally, the BTND boils down to an instance of joint non-negative matrix factorisation [50], [34], [31],
 [24] that takes on the following form:

$$\begin{aligned} \underset{\mathbf{F}, \mathbf{V}\{1\}, \dots, \mathbf{V}\{S\}}{\operatorname{argmin}} \quad & \sum_{s=1}^S \zeta_s \|\mathbf{X}\{s\} - \mathbf{F}\mathbf{V}\{s\}^t\|_F^2 + \lambda S \sum_{k=1}^K \sum_{l=1}^L |F_{lk}|, \\ \text{s.t.} \quad & C(\mathbf{V}_{:k}\{S\}, \gamma_s, \eta_s) \quad \forall k \in \{1, \dots, K\}, \quad \forall s \in \{1, \dots, S\}, \\ \text{s.t.} \quad & \mathbf{F} \geq 0, \quad \mathbf{V}\{s\} \geq 0 \quad \forall s \in \{1, \dots, S\}. \end{aligned} \quad (3)$$

117 The ζ_s are free parameters to balance the relative importance of each seizure (in our study, we consider all
 118 seizures evenly and select the ζ_s parameter according to the energy of each seizure, see the supplementary
 119 materials for more precision). The sparsity factor γ_s and the compactness factor η_s are chosen to adapt to
 120 the particular duration of each seizure s .

121 Then, the method is associated with three hyperparameters: λ and γ respectively controlling the **sparsity**
 122 level of the FC subgraphs and the activation profiles, and η regulating the temporal **compactness** of the
 123 activation profiles.

124 2.4 Additional comments on BTND

125 Let us stress that the optimisation problem of equation (3) is non-convex and therefore, different initial
 126 conditions yield different solutions corresponding to local maxima. As it is common practice for non-
 127 convex methods in machine learning (e.g. k -means for data clustering [23]), we repeatedly solve (3) with a
 128 different initialisation and retain the one that reached the smaller minimum cost function. In practice, we
 129 empirically chose 20 trials. As for the other hyper-parameters, we observed that $\eta = 0.2$ produces coherent

130 activation profiles. Also, fixing $\lambda = \gamma$ simplifies the procedure without altering the results significantly.
131 Then, λ is tuned so as to identify the 20% most resilient activated FC. To select the most pertinent number
132 of subgraphs, we successively compute the decomposition for K ranging from 3 to 10. Based on an
133 Elbow criterion and on visual inspection, we compare the quality of the resulting temporal activation and
134 subgraphs, identifying thus the best value for K . Finally, we normalize each subgraph such that their
135 connectivity strengths are between 0 and 1. We only retain connections above some threshold (empirically
136 set to 0.2 in our experiments) to eliminate non-significant interactions.

137 For more details on the practical use of the method, see the supplementary materials. We provide the
138 URL¹ for a Github repository with Matlab implementation of the proposed BNTD method.

3 APPLICATION ON A REAL DATASET OF EPILEPTIC PATIENTS

139 3.1 Patients

140 To illustrate the clinical relevance of the BNTD method, we applied the method on seizures recorded
141 with intracranial EEG in 9 epileptic patients.

142 We included 9 adult patients suffering from drug-resistant focal epilepsy, followed in the Department of
143 Functional Neurology and Epileptology at Lyon's University Hospital, who underwent intracranial EEG
144 with SEEG according to the following criteria: (i) at least 1 seizure recorded during long term monitoring ;
145 (ii) conventional visual analysis of the SEEG signals identified clearly the seizure-onset zone.

146 Clinical details of all the patient included are listed in table 1.

147 Among them, 8 patients presented seizures suggesting a temporal lobe involvement but with clinical
148 features or morphological alterations on brain MRI not typical for medial temporal epilepsy requiring
149 intracranial EEG. For one patient, clinical semiology suggested an involvement of operculo-insular cortex.
150 3 patients underwent surgical resection of the epileptogenic cortex and all had a good surgical outcome
151 (Engel class Ia for all patients with a follow-up duration between 4 months and 48 months). For 2 patients, a
152 focal thermolesion using SEEG electrodes was performed, resulting in a dramatic improvement of epilepsy
153 (Engel Ia for both patients with 4 and 5 months of follow-up). For 2 patients, surgery was contra-indicated
154 because of the involvement of both temporal lobes during seizures. For 2 patients, surgical resection is
155 planned based on SEEG findings but has not been performed at the time of the present study.

156 3.2 SEEG recordings

157 Intracerebral multi-contact electrodes (five-fifteen contacts, diameter 0.8 mm, length 2 mm and 1.5 mm
158 apart) were implanted according to Talairach's stereotactic method [22]. Electrode location was verified
159 with post-implantation MRI. Prolonged extra-operative recordings were performed to capture each patient's
160 habitual seizures.

161 SEEG data were acquired with a 256 channel video EEG monitoring system, Micromed video EEG
162 acquisition system (SD LTM express, Micromed, Treviso, Italy) using the following parameters: sampling
163 rate 256 Hz, high pass filter 0.15 Hz, low pass filter 200 Hz, notch filter at 50 Hz.

164 The median number of bipolar contacts recorded per patient was 101 (range 64-130). The main cerebral
165 structures targeted by intracranial electrodes for each patient are listed in the Supp. table S1. As a whole, for
166 all patients, the medial temporal lobe (anterior hippocampus, posterior hippocampus, amygdala, entorhinal
167 cortex), the temporal lateral neocortex and the insular cortex were always targeted. Depending on the
168 electroclinical findings of each patient, frontal lobe, parietal lobe and occipital cortex were targeted.

¹ <https://github.com/FrusqueGaetan/BTND>

169 For 9 patients, all available seizures were extracted, forming a dataset composed of a total of 27 seizures.
170 For 6 patients, 3 seizures were analyzed. For two patients, 4 seizures were analyzed and for one patient, a
171 single seizure was available for analysis. For each seizure, we extracted signals for at least 1 minute before
172 the onset of the seizure and the whole course of the seizure.

173 The duration of the seizure was largely heterogeneous both at the inter-individual and intra-individual
174 level. The median length of the seizures across patients was 96 s (range 18-337).

175 **3.3 SEEG signal analysis**

176 SEEG signals are considered in bipolar derivations; hence each signal is referenced to its closest neighbour.
177 A high pass filter, with a cut-off frequency equal to 20 Hz at -3dB was applied on SEEG signals in order to
178 highlight the high-frequency activity typical of seizure activity, particularly at seizure onset [5].

179 For each seizure, we computed the FC matrices during the pre-seizure period and the course of the
180 whole seizure using a classical connectivity measure, the Phase Locking Value (PLV) [33], [2]. Briefly, the
181 PLV quantifies the synchronization in phase between two signal. The phase of each signal is computed
182 by the Hilbert transform. The PLV is the time average of the relative phase difference. To compute the
183 FC matrices, the SEEG signals were windowed with four seconds sliding windows moving by steps of 1
184 second. For each four seconds window, the PLV between all pairs of bipolar contacts was computed to
185 produce the overall network at each time step.

186 Finally, the BTND method is applied to the set of several seizures for each patient, to decompose all
187 seizures in several subgraphs, activating through time.

188 **3.4 Comparison of network dynamics estimated through conventional visual analysis** 189 **and the BTND method**

190 Each seizure was pragmatically segmented in three main periods defined by visual analysis: seizure-onset,
191 seizure propagation and seizure ending. Visual analysis of the seizures was performed by an expert in
192 clinical SEEG interpretation (JJ). Seizure onset corresponded to the time period with a dramatic change of
193 SEEG signals with either low-voltage fast activity (typically above 20 Hz) or rhythmic spikes in a subset
194 of electrode contacts. Seizure propagation corresponded to an extended time period where ictal SEEG
195 discharge spread to several brain structures either locally or remotely from the seizure onset zone. The
196 recruitment of these regions in the propagation zone can happen either by independent activation of the
197 single areas or by activating multiple areas at the same time. Lastly, a seizure was supposed to have ended
198 when the activation across brain structures was mostly synchronous (typically synchronous spikes) and
199 stable in time and resolved ultimately.

200 For each time period, we determined the electrode contacts that were involved in the ictal wave with a
201 conventional visual inspection. The electrode contacts were then pooled in several anatomical predefined
202 subregions.

203 For each patient, the output of the BTND method provided the temporal profile of activation of several
204 common subgraphs of the whole network during each seizure. The list of activated subgraphs at each time
205 period of the seizure was then collected. Each subgraph included several contacts with strong functional
206 connectivity. At each time period, we determined which anatomical subregions were connected based on
207 the activated subgraphs.

208 Lastly, a qualitative comparison between the set of activated structures determined by visual analysis and
209 the BTND method was performed for each seizure. This study, involving human participants, was reviewed

210 and approved by CPP Lyon Sud EST IV (24/05/2012 N2012-A00516-37). The patients/participants
211 provided their written informed consent to participate in this study.

212 **3.5 Results for the real dataset of epileptic patients**

213 The overall functional connectivity organisation was extracted in all 27 seizures using the BTND method.
214 This means that the seizures (from 1 to 4) of one patient are processed together according to BNTD. Table 2
215 provides the qualitative comparison between the set of activated structures between visual analysis and
216 the BTND method for patient 1 and 2. As well, table 3 and 4 show the same qualitative comparison for
217 respectively patients 2-4 and patients 5-9.

218 Using this method, we found, in the case of 6 patients, that 6 distinct functional subgraphs characterised
219 the organisation of seizures; 7 subgraphs for 1 patient; 5 subgraphs for another one; and only 4 subgraphs
220 characterised seizures for the last patient. However, for each patient, some subgraphs were more strongly
221 activated before seizure onset or were continuously activated before seizure onset and remained active
222 during the course of the seizures. Those subgraphs were considered as non-specific subgraphs for the
223 ictal events. For 5 patients, 2 subgraphs were non-specific while for 4 patients a single subgraph was
224 non-specific.

225 At seizure onset, a single subgraph was activated for 1 patient, two subgraphs were activated for 4 patients,
226 three subgraphs were activated for 3 patients, and 5 subgraphs were activated for 1 patient. For 24 seizures
227 in 6 patients, the seizure onset determined by visual analysis overlapped closely with the network disclosed
228 by the BTND method. For those patients, the cortical regions underlying the seizure-onset zone determined
229 through visual analysis were included in the seizure-onset subgraphs. However, the seizure-onset subgraph
230 also included other regions with strong functional connectivity not directly outside of the seizure-onset
231 zone. For one of those 6 patients (Pt 2), the seizure involved either the left or the right medial temporal
232 lobe at seizure onset. The seizure-onset subgraph was different for each seizure, and the lateralisation
233 of the activated structures was concordant with visual analysis. For 3 seizures in one patient (Pt 9), the
234 seizure-onset subgraph was discordant from the seizure onset-zone. For this patient, the seizure-onset zone
235 involved either right or left medial temporal lobe depending on the seizure. The seizure-onset subgraph for
236 this patient was wrongly lateralised to the right or the left temporal lobe.

237 During seizure propagation, there was always a close spatial overlap between the activated subgraphs and
238 the brain regions involved at each part of the seizure in all patients. For the 27 seizures in the 9 patients,
239 the brain regions involved during seizure propagation were included in activated subgraphs. However,
240 the congruence between activated subgraphs and regions disclosed by visual analysis was not perfect: a
241 minority of regions were revealed by the BTND method but was not detected by visual analysis.

242 During seizure ending, a tight spatial overlap was also observed between activated subgraphs and brain
243 regions determined by visual analysis. For 23 seizures, the brain regions involved at seizure ending were
244 included in activated subgraphs. For 4 seizures in 1 patient, visual analysis disclosed more activated regions
245 than the BTND method (Pt 4).

246 The detailed results are now presented for two cases (Pt 1 and Pt 2)

247

248 **CASE 1:**

249 Pt 1 is a 49 years old male patient. Presurgical non invasive investigations suggested left temporal lobe
250 epilepsy but some radiological features were considered as atypical for mesial temporal lobe epilepsy
251 syndrome and prompted invasive EEG with SEEG. SEEG targeted several regions within left temporal
252 lobe (anterior hippocampus, posterior hippocampus, amygdala, temporal pole, anterior temporal neocortex,

253 posterior temporal lobe), left orbito frontal cortex, and right temporal lobe (right amygdala, right anterior
254 temporal neocortex).

255 Three seizures were recorded during SEEG. During the 3 seizures, the initial seizure-onset activity
256 developed in left anterior and posterior hippocampus with secondary involvement of the temporal pole,
257 amygdalar nucleus and left anterior temporal neocortex at the end of the seizures.

258 The BTND method applied to the three seizures decomposed the connectivity pattern in 6 subgraphs.
259 Figure 2 shows the recording of two seizures (seizure 1 and 2) of the Patient 1 for selected electrode contacts.
260 Below each recording, we provide the activation profiles of all subgraphs obtained by the BTND for this
261 specific seizure. On top is represented the main cerebral structures targeted by intracranial electrodes for
262 this patient. Figure 3 shows the 6 FC subgraphs revealed by the BTND.

263 One subgraph was active before the seizure and during the whole course of the seizures. This subgraph
264 was mostly composed of local connections within temporal lobe (mostly within anterior hippocampus,
265 posterior hippocampus, amygdala). At the seizure onset, during the first seconds of the seizure, there was a
266 reproducible activation of one subgraph, that involved mostly connections between anterior hippocampus
267 and amygdala, posterior hippocampus and posterior temporal neocortex. A few seconds later, a strong
268 activation of another subgraph was observed, that involved mostly connections between medial temporal
269 lobe and temporal pole. During the course of the seizures, there was a consistent activation of three other
270 subgraphs, with a very similar pattern between seizures. Those subgraphs contained mostly connections
271 between anterior lateral temporal neocortex, temporal posterior neocortex, and temporal pole. As a whole,
272 the pattern of activations was very similar for the three seizures and was very consistent with visual analysis
273 of the seizures.

274 From a clinical point of view, at seizure onset, the patient was asymptomatic and the seizure remained
275 clinically silent for almost 80 s. First clinical symptoms (behavioral arrest and loss of consciousness)
276 occurred more than 1 minute after seizure onset during the course propagation. Secondary clinical
277 manifestations included oro alimentary automatisms (seizure 1) and right arm dystonia (seizure 2). Those
278 symptoms occurred while several modules were simultaneously activated.

279 The patient underwent left anterior lobectomy that resulted in seizure freedom with more than 24 months
280 of follow-up.

281

282

283 **CASE 2:**

284 Pt 2 is a 37 years old female patient. Presurgical non invasive investigations suggested that both temporal
285 lobes could trigger habitual epileptic seizures of the patient. Intracranial EEG using SEEG was thus
286 required to evaluate the intrinsic epileptogenicity of each temporal lobe. Intracranial SEEG electrodes
287 targeted mostly both medial and lateral temporal lobes (left and right anterior hippocampus, left and right
288 temporal pole, right amygdala, left and right anterior temporal neocortex, left and right posterior temporal
289 neocortex, left and right insula), but also left and right orbitofrontal cortex.

290 Three seizures were recorded during SEEG. For the seizure 1, seizure-onset was characterised by a
291 rapid discharge in the left anterior and posterior hippocampus with secondary spread to left anterior lateral
292 temporal and left orbito frontal cortex fast activity and at the end of the seizure propagation to right temporal
293 lobe (right hippocampus and right amygdala). For two seizures (seizure 2 and 3), the initial seizure-onset
294 activity developed in right hippocampus, right amygdala and right entorhinal cortex with a secondary ictal
295 spread to right anterior temporal cortex and with a propagation to left temporal lobe at seizure ending.

296 The BTND method applied to the three seizures decomposed the connectivity pattern in 7 subgraphs.
297 Figure ?? shows the recording of two seizures (seizure 1 and 2) of the Patient 2 for selected electrode
298 contacts. Below each recording, we provide the activation profiles of all subgraphs obtained by the BTND
299 for this specific seizure. On top is represented the main cerebral structures targeted by intracranial electrodes
300 for this patient. Figure 5 shows the 7 FC subgraphs revealed by the BTND.

301 One subgraph was mostly composed of connections within left medial temporal lobe and left orbitofrontal
302 cortex. Another subgraph was mostly composed of connections within left anterior temporal neocortex.
303 The remaining five subgraphs consisted of regions connecting mostly right medial temporal structures
304 (hippocampus, amygdala, entorhinal cortex) and/or right lateral temporal neocortex. The time course of
305 activation of those subgraphs was closely related to the ictal involvement of both temporal lobes revealed
306 by visual analysis of the seizures: involvement of the left (right) medial temporal lobe was paralleled by an
307 activation of the left (right) subgraphs in a timely fashion, depending on the seizure.

308 Clinically, ictal semiology for seizure 1 consisted in nausea and olfactory hallucinations with preserved
309 consciousness reported consciously by the patient 30 seconds after EEG onset followed by behavioral arrest
310 with loss of consciousness more 60 seconds later. Loss of consciousness occurred lately during the course
311 of the seizure when both temporal lobes were involved. At that time, the BTND method showed activation
312 of modules in both temporal lobes. Seizure 2 was a nocturnal seizure with mild clinical semiology, mostly
313 consisting in nocturnal arousal and confusion.

314 Since SEEG revealed an intrinsic epileptogenicity of both temporal lobes, surgical resection was contra-
315 indicated.

4 DISCUSSION

316 This study investigated a new method named BTND to decompose the multi-seizure brain-wide time-
317 varying network obtained by means of Functional Connectivities. The dataset is visualised as FC sub-
318 graphs characterising the dynamic of all seizures from the same patient. The FC measure used was
319 the PLV, estimated at different time steps of the seizure and applied on large band signal (20-100 Hz).
320 We compared the obtained decomposition of ictal events from 9 patients who have drug-resistant focal
321 epilepsy (observation of a total of 27 seizures), to the visual interpretation from the clinician. Overall, for
322 every patient, results consisting of spatially localised FC subgraphs with stepwise activation were easily
323 interpretable. For 8 of the 9 patients, the decomposition matched with the clinical observation entailing the
324 BTND method as a relevant tool to visualise the multi-seizure brain-wide time-varying network.

325 4.1 Investigating seizure dynamics with brain-wide time-varying network

326 It is well established that the brain is a complex network, with a sophisticated structural connectivity
327 architecture and specific anatomical networks shaping sensory and cognitive processes [9], [45]. Functional
328 connectivity measures are a statistical way to investigate the interrelations between brain regions, forming
329 a physiological or pathological brain network [20]. When applied on static processes, FC network analysis
330 can provide an instantaneous picture of a stable network. In the field of clinical neuroscience, this proved
331 to be useful for studying stable disease traits like the effects of specific lesions [43] or the effects of drugs
332 on the brain [19], [16], [1]. Graph theory-based measures can then provide quantitative tools to explore
333 the overall topology of the network [45]. Thus, specific metrics like modularity, clustering coefficients or
334 efficiency originating from graph theory [10] were proposed as a useful strategy, for example, to classify
335 patients with Alzheimer disease from standard patients [41] or to explain the effect of physical activity on
336 relations between brain regions [26].

337 However, static network analysis does not capture one fundamental property of epileptic seizures, the
338 dynamic propagation of the ictal wave. Analysis of time-varying network inferred by dynamic FC measures
339 is a recent topic. Newly emerging dynamic measures which quantify how community organisation evolved
340 in time have been proposed in recent years [30]. In this context, [27] shows that simple metrics using
341 the first eigenvector of each FC network lead to the separation of ictal, pre-ictal or non-ictal events of a
342 recording. A similar metric demonstrated in [11] used to describe the seizure as a succession of states.
343 The strategy can be used to decompose the time axes in states, and then to extract the major FC network
344 of each state [37]. Despite producing intelligible results, this strategy hampers the identification of FC
345 subgraphs with interconnected temporal activation, and prevents highlighting some complex relations
346 between brain regions. A complementary approach has been proposed in [29]: the authors identify first
347 the main subgraphs of the seizures by modularity optimisation [39], and the evolution in time of the main
348 subgraphs leads to a decomposition of the seizure in time states. It should be noticed that this approach is
349 not fundamentally different from the study of static graphs since the subgraphs and their time evolution
350 are determined independently. However, in addition to finding a measure characterising each FC graph,
351 one must know how to analyse the temporal evolution of the proposed scores. It becomes even more
352 complicated when several modalities are used, as in [35], where several seizures are analysed for different
353 frequency bands over time.

354 The present study proposes another strategy, consisting of decomposing all modalities characterising the
355 dataset simultaneously. Thus, the main advantages of the proposed method are that the analysis pipeline
356 provides both the subgraphs and their temporal activations. The output of the process highlights the
357 main components of the connectivity structure and summarises a large amount of data with an automatic
358 approach. A similar approach has already been employed in the context of epilepsy in [28] to decompose
359 FC matrices from seizures into FC subgraphs with their respective activation profile. Khambhati and
360 colleagues [28] demonstrate that inferred FC subgraphs during interictal periods can predict brain regions
361 that generate seizures, and that those subgraphs undergo slower and more coordinated fluctuations during
362 the ictal events compared to interictal states. However, this kind of simultaneous decompositions can
363 produce results that are difficult to interpret. Therefore, for an application different from epilepsy, a sparsity
364 constraint applied on activation profile was shown to enforce intelligibility of the results [12], providing
365 FC subgraphs discriminating the brain network's dynamic in neurodevelopment. Moreover, contrary to our
366 study, the decomposition from [28] does not integrate the different seizures of the same patient to obtain
367 more reproducible FC subgraphs. Tools to decompose several modalities, like tensor decomposition [14],
368 [32], [15], were already applied in neuroscience [36], [37], [40] and recently in the context of epilepsy [17].
369 In [17], we proposed a specific tensor decomposition with relevant constraints to encourage the inference
370 of interpretable clusters of FC common to several seizures of the same patient. However, this method
371 is only applicable if all seizures from the same patient have similar durations. In the present study, we
372 developed a new method offering the possibility of decomposing several seizures with different durations
373 from the same patient, which is a more realistic situation in a clinical setting.

374 4.2 Limitations

375 The BTND method can produce relevant FC , but several limitations have to be addressed. First, the
376 method requires 3 parameters that are directly related to the obtained FC results. We expose a simple
377 procedure to choose each parameter that produces relevant results for each of the 27 seizures. However, the
378 optimal selection of these parameters may be dependant of the FC measure and might be adapted for other
379 clinical applications. Secondly, for one patient, the BTND method identified a seizure-onset subgraph that
380 was discordant from the seizure onset-zone. For that patient, at seizure-onset, there was a rapid discharge
381 within the seizure-onset zone (without any focal change of synchrony) and a spiking activity within the

382 contralateral hemisphere (accompanied with an increase of synchrony). The increase of FC evaluated by
383 the phase-locking value was wrongly lateralised, emphasising that the BTND method is dependant of the
384 FC measure used to infer the brain-wide time-varying network. Thus, using another FC measure could
385 be envisaged for this patient. In addition, several studies have already shown that seizure-onset is often
386 marked by a dramatic decrease in seizure connectivity among recorded brain structures. At the same time,
387 synchrony increases progressively during the seizure [52], [25]. It might be thus expected that seizure-onset
388 should be characterised by a decrease of activation of subgraphs located within the seizure-onset zone with
389 the BTND method in some patients. It is important to consider that our procedure only highlights functional
390 subgraphs associated with high values of functional connectivity. Thus, it is ideal for showing activations of
391 synchrony in different areas of the brain. However, it is not able to explicitly demonstrate the deactivations
392 that may occur in the brain at the early start of the seizure when SEEG activities in different areas of the
393 brain are suddenly decorrelated. Lastly, direct validation of the method is out of reach since there is no
394 perfect gold-standard for the estimation of the connectivity pattern in epileptic patients. We chose to make
395 a correspondence between the propagation patterns disclosed by classical visual interpretation of SEEG
396 signals and the BTND method. Simulation studies generating neural models of epileptic activity with a
397 known connectivity pattern could represent an alternative in future studies.

398 **4.3 Clinical application of the method**

399 In the present study, we presented an automatic method to describe the connectivity structures of epileptic
400 seizures using an original algorithm with several constraints optimized for that clinical context.

401 As a whole, we found that the method produces several subgraphs of connections with their activation
402 time course that parallel the patterns of propagation of the seizures closely. In 24/27 seizures, one or two
403 subgraphs overlapped clearly with the seizure onset zone. This suggests that the method can help to localize
404 the seizure-onset zone if there is an increase of synchrony at seizure-onset revealed by FC. This finding
405 confirms several studies evidencing that focal modulations of synchrony helps to localise the seizure-onset
406 zone to be surgically resected [49], [7]. Moreover, thanks to the sparsity and temporal coherence constraints,
407 the method effortlessly reveals how FC synchrony propagates to the different regions of the brain. As a
408 whole, the method summarises a vast amount of complex interactions with high readability. We believe
409 that the method is thus highly valuable in clinical studies focusing on connectivity in epileptic patients.
410 For example, this may help to unravel the neural bases of clinical semiology of seizures, which are often
411 related to ictal dysfunction of widespread brain networks involving cortical or subcortical structures.
412 The BTND method provides an exhaustive view of the structure of functional networks at each period
413 of the seizure enabling a fine-grained correlation ictal semiology and network analysis. Lastly, clinical
414 interpretation of SEEG signals is mostly focussed on changes of power in large frequency bands (typically
415 high-frequency above 20 Hz at seizure-onset and low band or large band frequency during propagation)
416 revealed by visual inspection. The BTND method enables the detection of changes of synchrony revealed
417 by functional connectivity measures which are not necessarily paralleled by changes of power. In that
418 respect, we believe that the method may thus contribute to bringing into clinical practice computational
419 measures complementary to a visual interpretation of seizures.

5 CONCLUSION

420 We present here a novel approach to decompose epileptic seizures in several time-varying subgraphs with
421 high and reproducible functional connectivity values. The method extracts the most significant subgraphs
422 and their corresponding time-course of activation. We suggest that this represents a first step to simplify
423 the interpretation of large datasets of functional connectivity for clinical practice. We believe that this will
424 enable further studies investigating the clinical relevance of networks identification for epilepsy surgery.

CONFLICT OF INTEREST STATEMENT

425 The authors declare that the research was conducted in the absence of any commercial or financial
426 relationships that could be construed as a potential conflict of interest.

AUTHOR CONTRIBUTIONS

427 GF: concept, method design, data analysis, bibliographic review, writing contributions to the manuscript
428 introduction, material and methods and discussion, submission. PB: critical review of the manuscript,
429 scientific supervision (data analysis). PG: critical review of the manuscript, scientific supervision (data
430 analysis). JJ: concept, experiment design, scientific supervision (clinic), bibliographic review, writing
431 contributions to the manuscript introduction, application and discussion.

FUNDING

432 This work was supported by the ACADEMICS grant of the IDEXLYON, project of the Université de Lyon,
433 PIA operated by ANR-16-IDEX-0005.

SUPPLEMENTAL DATA

434 The Supplementary Material for this article can be found online at: Supplementary Material

REFERENCES

- 435 [1]Joan F. Alonso, Miguel A. Mañanas, Sergio Romero, Dirk Hoyer, Jordi Riba, and Manel J. Barbanøj.
436 Drug effect on EEG connectivity assessed by linear and nonlinear couplings. *Human brain mapping*,
437 31(3):487–497, 2010.
- 438 [2]Sergul Aydore, Dimitrios Pantazis, and Richard M. Leahy. A note on the phase locking value and its
439 properties. *Neuroimage*, 74:231–244, 2013.
- 440 [3]F. Bartolomei, G. Bettus, C. J. Stam, and M. Guye. Interictal network properties in mesial temporal
441 lobe epilepsy: a graph theoretical study from intracerebral recordings. *Clinical neurophysiology*,
442 124(12):2345–2353, 2013. ISBN: 1388-2457 Publisher: Elsevier.
- 443 [4]Fabrice Bartolomei, Emmanuel J. Barbeau, Trung Nguyen, Aileen McGonigal, Jean Régis, Patrick
444 Chauvel, and Fabrice Wendling. Rhinal-hippocampal interactions during déjà vu. *Clinical*
445 *Neurophysiology: Official Journal of the International Federation of Clinical Neurophysiology*,
446 123(3):489–495, March 2012. Number: 3.
- 447 [5]Fabrice Bartolomei, Patrick Chauvel, and Fabrice Wendling. Epileptogenicity of brain structures
448 in human temporal lobe epilepsy: a quantified study from intracerebral EEG. *Brain: A Journal of*
449 *Neurology*, 131(Pt 7):1818–1830, July 2008. Number: Pt 7.
- 450 [6]Fabrice Bartolomei, Martine Gavaret, Russell Hewett, Luc Valton, Sandrine Aubert, Jean Régis,
451 Fabrice Wendling, and Patrick Chauvel. Neural networks underlying parietal lobe seizures: a quantified
452 study from intracerebral recordings. *Epilepsy Research*, 93(2-3):164–176, February 2011. Number:
453 2-3.
- 454 [7]Fabrice Bartolomei, Stanislas Lagarde, Fabrice Wendling, Aileen McGonigal, Viktor Jirsa, Maxime
455 Guye, and Christian Bénar. Defining epileptogenic networks: Contribution of SEEG and signal analysis.
456 *Epilepsia*, 58(7):1131–1147, 2017. Number: 7.
- 457 [8]Fabrice Bartolomei, Agnes Trébuchon, Martine Gavaret, Jean Régis, Fabrice Wendling, and Patrick
458 Chauvel. Acute alteration of emotional behaviour in epileptic seizures is related to transient
459 desynchrony in emotion-regulation networks. *Clinical Neurophysiology: Official Journal of the*

- 460 *International Federation of Clinical Neurophysiology*, 116(10):2473–2479, October 2005. Number:
461 10.
- 462 [9]Danielle S. Bassett and Olaf Sporns. Network neuroscience. *Nature Neuroscience*, 20(3):353–364,
463 February 2017. Number: 3.
- 464 [10]Ed Bullmore and Olaf Sporns. Complex brain networks: graph theoretical analysis of structural and
465 functional systems. *Nature reviews neuroscience*, 10(3):186–198, 2009.
- 466 [11]Samuel P. Burns, Sabato Santaniello, Robert B. Yaffe, Christophe C. Jouny, Nathan E. Crone,
467 Gregory K. Bergey, William S. Anderson, and Sridevi V. Sarma. Network dynamics of the brain
468 and influence of the epileptic seizure onset zone. *Proceedings of the National Academy of Sciences*,
469 111(49):E5321–E5330, 2014.
- 470 [12]Lucy R. Chai, Ankit N. Khambhati, Rastko Ciric, Tyler M. Moore, Ruben C. Gur, Raquel E.
471 Gur, Theodore D. Satterthwaite, and Danielle S. Bassett. Evolution of brain network dynamics
472 in neurodevelopment. *Network Neuroscience*, 1(1):14–30, 2017.
- 473 [13]Patrick Chauvel, Jorge Gonzalez-Martinez, and Juan Bulacio. Presurgical intracranial investigations in
474 epilepsy surgery. *Handbook of Clinical Neurology*, 161:45–71, 2019.
- 475 [14]Andrzej Cichocki. Tensor decompositions: a new concept in brain data analysis? *arXiv preprint*
476 *arXiv:1305.0395*, 2013.
- 477 [15]Pierre Comon. Tensors: a brief introduction. *IEEE Signal Processing Magazine*, 31(3):44–53, 2014.
- 478 [16]Linda Douw, Edwin van Dellen, Alida A. Gouw, Alessandra Griffa, Willem de Haan, Martijn van den
479 Heuvel, Arjan Hillebrand, Piet Van Mieghem, Ida A. Nissen, Willem M. Otte, Yael D. Reijmer,
480 Menno M. Schoonheim, Mario Senden, Elisabeth C. W. van Straaten, Betty M. Tijms, Prejaas Tewarie,
481 and Cornelis J. Stam. The road ahead in clinical network neuroscience. *Network Neuroscience*
482 *(Cambridge, Mass.)*, 3(4):969–993, 2019. Number: 4.
- 483 [17]Gaëtan Michel Frusque, Julien Jung, Pierre Borgnat, and Paulo Gonçalves. Multiplex network
484 inference with sparse tensor decomposition for functional connectivity. *IEEE transactions on Signal*
485 *and Information Processing over Networks*, 2020. ISBN: 2373-776X Publisher: IEEE.
- 486 [18]Marc Guenet, Jean Isnard, Philippe Ryvlin, Catherine Fischer, Karine Ostrowsky, François Mauguier,
487 and Marc Sindou. Neurophysiological monitoring for epilepsy surgery: the Talairach SEEG method.
488 *Stereotactic and functional neurosurgery*, 77(1-4):29–32, 2001.
- 489 [19]Mark Hallett, Willem de Haan, Gustavo Deco, Reinhard Dengler, Riccardo Di Iorio, Cecile Gallea,
490 Christian Gerloff, Christian Grefkes, Rick C. Helmich, Morten L. Kringelbach, Francesca Miraglia,
491 Ivan Rektor, Ondřej Strýček, Fabrizio Vecchio, Lukas J. Volz, Tao Wu, and Paolo M. Rossini. Human
492 brain connectivity: Clinical applications for clinical neurophysiology. *Clinical Neurophysiology:*
493 *Official Journal of the International Federation of Clinical Neurophysiology*, 131(7):1621–1651, July
494 2020. Number: 7.
- 495 [20]Bin He, Laura Astolfi, Pedro A. Valdes-Sosa, Daniele Marinazzo, Satu Palva, Christian G. Benar,
496 Christoph M. Michel, and Thomas Koenig. Electrophysiological Brain Connectivity: Theory and
497 Implementation. *IEEE transactions on bio-medical engineering*, May 2019.
- 498 [21]Seok-Jun Hong, Boris C. Bernhardt, Ravnoor S. Gill, Neda Bernasconi, and Andrea Bernasconi. The
499 spectrum of structural and functional network alterations in malformations of cortical development.
500 *Brain*, 140(8):2133–2143, 2017. ISBN: 0006-8950 Publisher: Oxford University Press.
- 501 [22]Jean Isnard, Delphine Taussig, Fabrice Bartolomei, Pierre Bourdillon, Hélène Catenoix, Francine
502 Chassoux, Mathilde Chipaux, Stéphane Clemenceau, Sophie Colnat-Coulbois, and Marie Denuelle.
503 French guidelines on stereoelectroencephalography (SEEG). *Neurophysiologie Clinique*, 48(1):5–13,
504 2018.

- 505 [23]Anil K. Jain. Data clustering: 50 years beyond K-means. *Pattern recognition letters*, 31(8):651–666,
506 2010.
- 507 [24]Xingpeng Jiang, Xiaohua Hu, and Weiwei Xu. Microbiome data representation by joint nonnegative
508 matrix factorization with laplacian regularization. *IEEE/ACM transactions on computational biology
509 and bioinformatics*, 14(2):353–359, 2015.
- 510 [25]Premysl Jiruska, Marco de Curtis, John G. R. Jefferys, Catherine A. Schevon, Steven J. Schiff, and
511 Kaspar Schindler. Synchronization and desynchronization in epilepsy: controversies and hypotheses.
512 *The Journal of Physiology*, 591(4):787–797, February 2013. Number: 4.
- 513 [26]Keita Kamijo, Yuji Takeda, and Charles H. Hillman. The relation of physical activity to functional
514 connectivity between brain regions. *Clinical Neurophysiology*, 122(1):81–89, 2011.
- 515 [27]Matthew SD Kerr, Samuel P. Burns, John Gale, Jorge Gonzalez-Martinez, Juan Bulacio, and Sridevi V.
516 Sarma. Multivariate analysis of SEEG signals during seizure. In *2011 Annual International Conference
517 of the IEEE Engineering in Medicine and Biology Society*, pages 8279–8282. IEEE, 2011.
- 518 [28]Ankit N. Khambhati, Danielle S. Bassett, Brian S. Oommen, Stephanie H. Chen, Timothy H. Lucas,
519 Kathryn A. Davis, and Brian Litt. Recurring functional interactions predict network architecture of
520 interictal and ictal states in neocortical epilepsy. *eneuro*, 4(1), 2017.
- 521 [29]Ankit N. Khambhati, Kathryn A. Davis, Brian S. Oommen, Stephanie H. Chen, Timothy H. Lucas,
522 Brian Litt, and Danielle S. Bassett. Dynamic network drivers of seizure generation, propagation and
523 termination in human neocortical epilepsy. *PLoS computational biology*, 11(12), 2015.
- 524 [30]Ankit N. Khambhati, Ann E. Sizemore, Richard F. Betzel, and Danielle S. Bassett. Modelling And
525 Interpreting Network Dynamics. *bioRxiv*, page 124016, 2017.
- 526 [31]Hannah Kim, Jaegul Choo, Jingu Kim, Chandan K. Reddy, and Haesun Park. Simultaneous discovery
527 of common and discriminative topics via joint nonnegative matrix factorization. In *Proceedings of
528 the 21th ACM SIGKDD International Conference on Knowledge Discovery and Data Mining*, pages
529 567–576, 2015.
- 530 [32]T. Kolda and B. Bader. Tensor Decompositions and Applications. *SIAM Review*, 51(3):455–500,
531 August 2009.
- 532 [33]J. P. Lachaux, E. Rodriguez, J. Martinerie, and F. J. Varela. Measuring phase synchrony in brain
533 signals. *Human Brain Mapping*, 8(4):194–208, 1999. Number: 4.
- 534 [34]Preethi Lahoti, Kiran Garimella, and Aristides Gionis. Joint non-negative matrix factorization for
535 learning ideological leaning on twitter. In *Proceedings of the Eleventh ACM International Conference
536 on Web Search and Data Mining*, pages 351–359, 2018.
- 537 [35]Michel Le Van Quyen, Jason Soss, Vincent Navarro, Richard Robertson, Mario Chavez, Michel
538 Baulac, and Jacques Martinerie. Preictal state identification by synchronization changes in long-term
539 intracranial EEG recordings. *Clinical Neurophysiology*, 116(3):559–568, 2005.
- 540 [36]Nora Leonardi and Dimitri Van De Ville. Identifying network correlates of brain states using
541 tensor decompositions of whole-brain dynamic functional connectivity. In *Pattern Recognition
542 in Neuroimaging (PRNI), 2013 International Workshop on*, pages 74–77. IEEE, 2013.
- 543 [37]Arash Golibagh Mahyari, David M. Zoltowski, Edward M. Bernat, and Selin Aviyente. A Tensor
544 Decomposition-Based Approach for Detecting Dynamic Network States From EEG. *IEEE Transactions
545 on Biomedical Engineering*, 64(1):225–237, 2017.
- 546 [38]Julien Mairal, Francis Bach, Jean Ponce, and Guillermo Sapiro. Online learning for matrix factorization
547 and sparse coding. *Journal of Machine Learning Research*, 11(Jan):19–60, 2010.
- 548 [39]Mark Newman. *Networks*. Oxford university press, 2018.

- 549 [40]Alp Ozdemir, Edward M. Bernat, and Selin Aviyente. Recursive tensor subspace tracking for dynamic
550 brain network analysis. *IEEE Transactions on Signal and Information Processing over Networks*,
551 3(4):669–682, 2017.
- 552 [41]Mikhail Rubinov, Stuart A. Knock, Cornelis J. Stam, Sifis Micheloyannis, Anthony WF Harris,
553 Leanne M. Williams, and Michael Breakspear. Small-world properties of nonlinear brain activity in
554 schizophrenia. *Human brain mapping*, 30(2):403–416, 2009.
- 555 [42]Philippe Ryvlin, J. Helen Cross, and Sylvain Rheims. Epilepsy surgery in children and adults. *The
556 Lancet. Neurology*, 13(11):1114–1126, November 2014. Number: 11.
- 557 [43]Scott R. Sponheim, Kathryn A. McGuire, Seung Suk Kang, Nicholas D. Davenport, Selin Aviyente,
558 Edward M. Bernat, and Kelvin O. Lim. Evidence of disrupted functional connectivity in the brain after
559 combat-related blast injury. *Neuroimage*, 54:S21–S29, 2011.
- 560 [44]William Stacey, Mark Kramer, Kristin Gunnarsdottir, Jorge Gonzalez-Martinez, Kareem Zaghoul,
561 Sara Inati, Sridevi Sarma, Jennifer Stiso, Ankit N. Khambhati, Danielle S. Bassett, Rachel J. Smith,
562 Virginia B. Liu, Beth A. Lopour, and Richard Staba. Emerging roles of network analysis for epilepsy.
563 *Epilepsy Research*, 159:106255, January 2020.
- 564 [45]Cornelis J. Stam. Modern network science of neurological disorders. *Nature Reviews. Neuroscience*,
565 15(10):683–695, October 2014. Number: 10.
- 566 [46]Martijn P. van den Heuvel and Olaf Sporns. A cross-disorder connectome landscape of brain
567 dysconnectivity. *Nature Reviews. Neuroscience*, 20(7):435–446, 2019. Number: 7.
- 568 [47]Pieter Van Mierlo, Evelien Carrette, Hans Hallez, Robrecht Raedt, Alfred Meurs, Stefaan
569 Vandenberghe, Dirk Van Roost, Paul Boon, Steven Staelens, and Kristl Vonck. Ictal-onset localization
570 through connectivity analysis of intracranial EEG signals in patients with refractory epilepsy. *Epilepsia*,
571 54(8):1409–1418, 2013. ISBN: 0013-9580 Publisher: Wiley Online Library.
- 572 [48]Pieter van Mierlo, Yvonne Höller, Niels K. Focke, and Serge Vulliemoz. Network Perspectives on
573 Epilepsy Using EEG/MEG Source Connectivity. *Frontiers in Neurology*, 10:721, 2019.
- 574 [49]Pieter van Mierlo, Margarita Papadopoulou, Evelien Carrette, Paul Boon, Stefaan Vandenberghe, Kristl
575 Vonck, and Daniele Marinazzo. Functional brain connectivity from EEG in epilepsy: seizure prediction
576 and epileptogenic focus localization. *Progress in Neurobiology*, 121:19–35, October 2014.
- 577 [50]Hong-Qiang Wang, Chun-Hou Zheng, and Xing-Ming Zhao. j NMFMA: a joint non-negative matrix
578 factorization meta-analysis of transcriptomics data. *Bioinformatics*, 31(4):572–580, 2015.
- 579 [51]Meng-yang Wang, Jing Wang, Jian Zhou, Yu-guang Guan, Feng Zhai, Chang-qing Liu, Fei-fei Xu,
580 Yi-xian Han, Zhao-fen Yan, and Guo-ming Luan. Identification of the epileptogenic zone of temporal
581 lobe epilepsy from stereo-electroencephalography signals: A phase transfer entropy and graph theory
582 approach. *NeuroImage: Clinical*, 16:184–195, 2017. ISBN: 2213-1582 Publisher: Elsevier.
- 583 [52]Fabrice Wendling, Fabrice Bartolomei, Jean-Jacques Bellanger, Jérôme Bourien, and Patrick Chauvel.
584 Epileptic fast intracerebral EEG activity: evidence for spatial decorrelation at seizure onset. *Brain*,
585 126(6):1449–1459, 2003.
- 586 [53]Christopher Wilke, Wim Van Drongelen, Michael Kohrman, and Bin He. Neocortical seizure foci
587 localization by means of a directed transfer function method. *Epilepsia*, 51(4):564–572, 2010. ISBN:
588 0013-9580 Publisher: Wiley Online Library.

FIGURE CAPTIONS AND TABLES

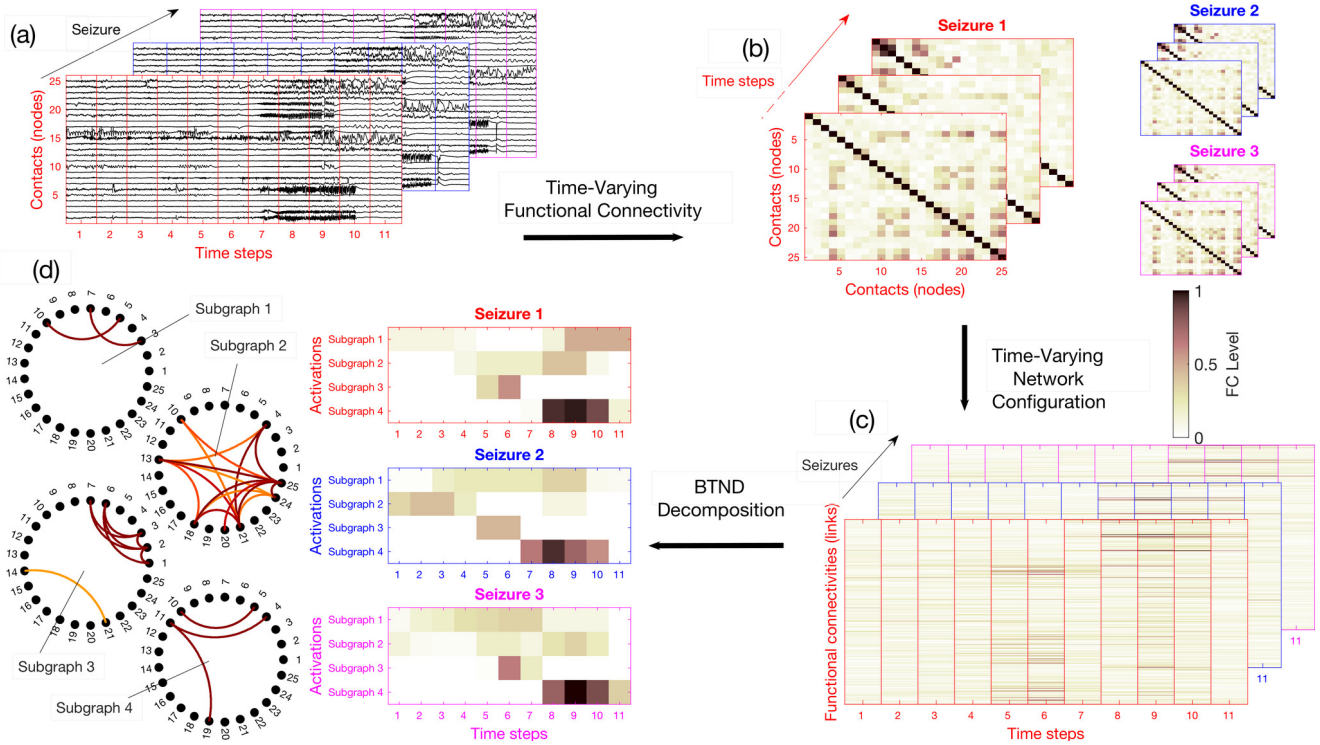


Figure 1. Overview of the strategy: (a) We chop each recording in time segment, potentially with some overlapping. (b) For each segment, we compute the connectivity level of each pair of electrode contacts with an FC measure. (c) We rearrange the FC measures in a vector, stacked in time they form for each seizure an FC matrix. (d) the list of FC matrix is decomposed into a set of FC graphs with their activation profiles respective to each seizure. Here, the number of subgraph is $K = 4$, the activation profiles of each subgraph are represented for the 3 available seizures of this patient.

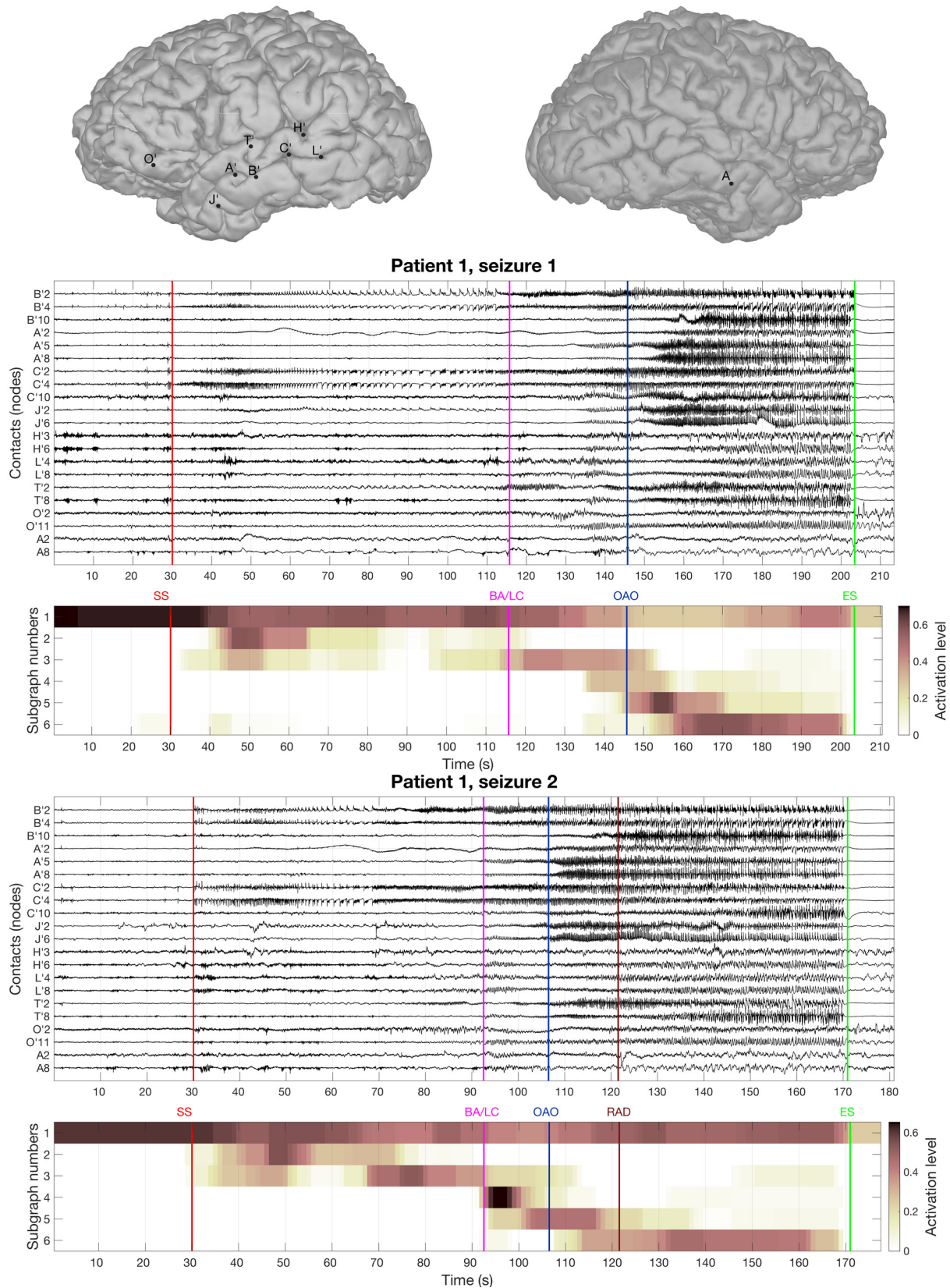


Figure 2. On top is represented the main cerebral structures targeted by intracranial electrodes for patient 1. Then we picture the recording of two seizures of the Patient 1 for selected electrode contacts. Under each seizure, we show the activation level of each subgraph obtained by the BTND decomposition. A subgraph is composed of pairs of contacts with high FC values. The activation level shows the FC dynamic of a subgraph. The main features of ictal semiology are represented by vertical lines, SS=start of the seizure, BA/LC=clinical onset with behavioural arrest and loss of consciousness, OAO=oro alimentary automatisms, RAD=right arm dystonia, SE=end of the seizure. **17**

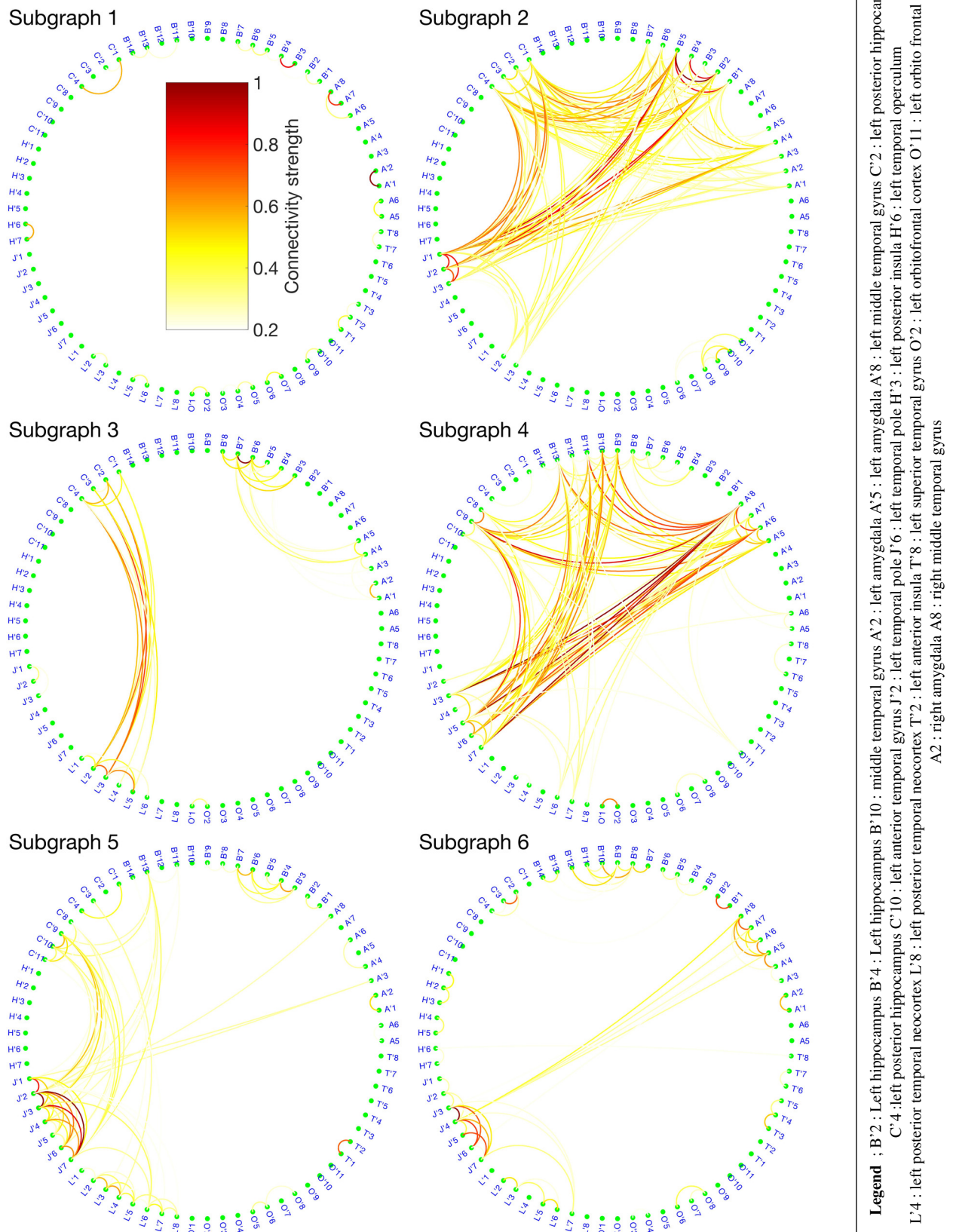


Figure 3. 6 FC subgraphs revealed by the BTND decomposition for the patient 1. The colorbar is the same for each graph. Only the electrode contacts that show one or several connections in at least one subgraph are represented.

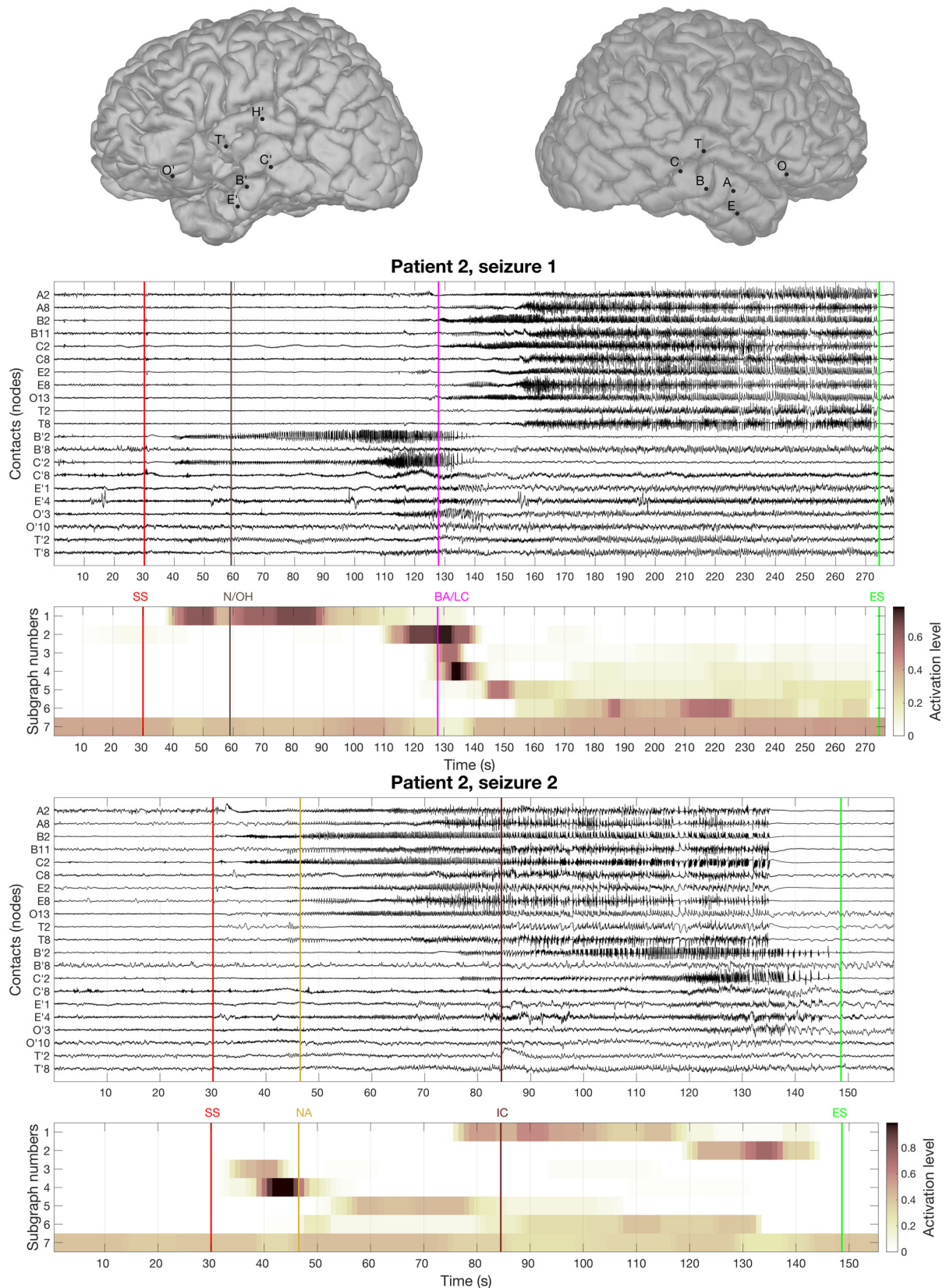


Figure 4. On top is represented the main cerebral structures targeted by intracranial electrodes for patient 2. Then we picture the recording of two seizures of the Patient 2 for selected electrode contacts. Under each seizure, we show the activation level of each subgraph obtained by the BTND decomposition. A subgraph is composed of pairs of contacts with high FC values. The activation level shows the FC dynamic of a subgraph. The main features of ictal semiology are represented by vertical lines, BA/LC=behavioural arrest and loss of consciousness, N/OH=clinical onset with nausea and olfactory hallucinations, NA=nocturnal arousal, IC=ictal confusion.

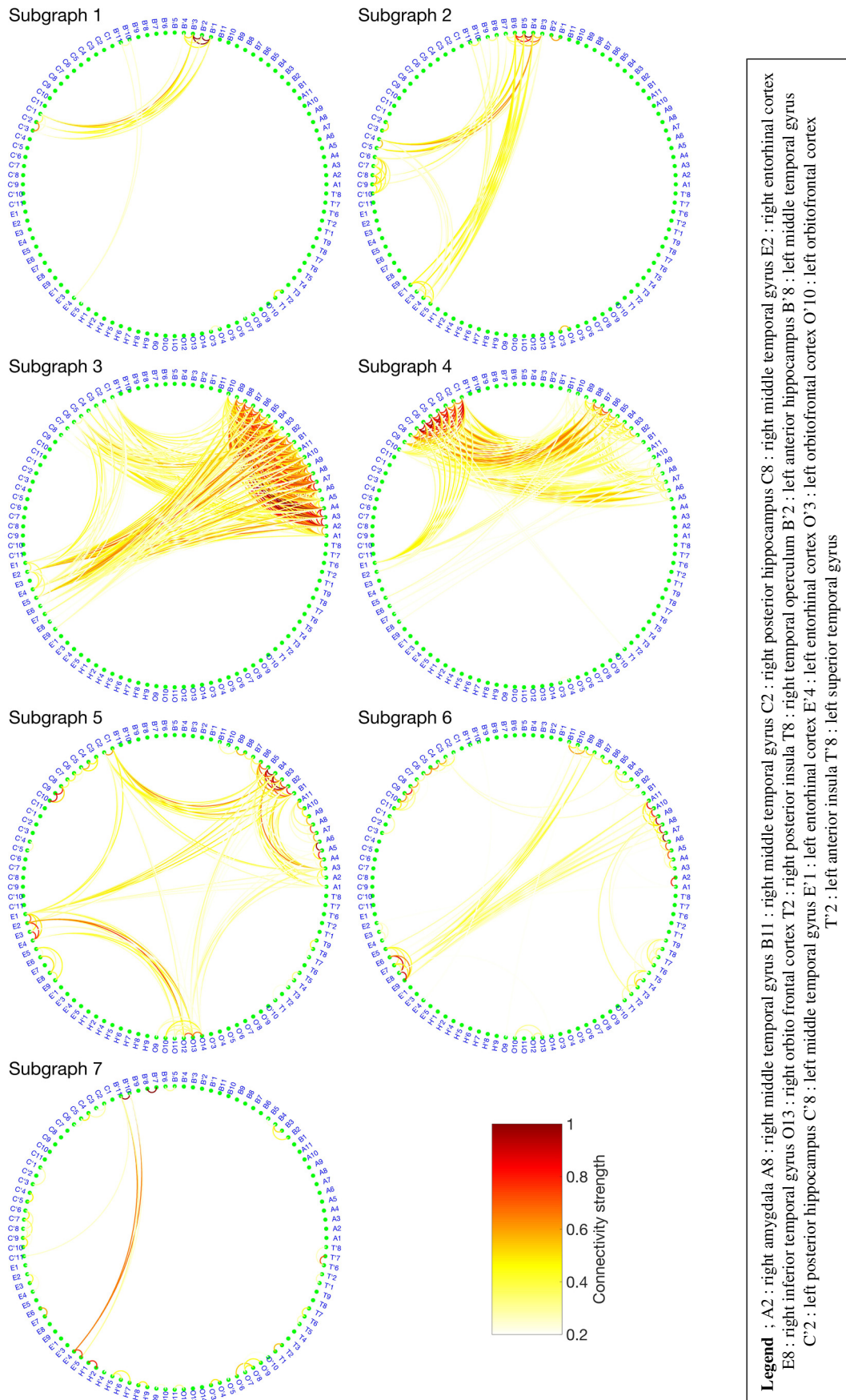


Figure 5. 7 FC subgraphs revealed by the BTND decomposition for the patient 2. Only the electrode contacts that show one or several connections in at least one subgraph are represented.

| Patient | BRAIN MRI | INTERICTAL EEG | ICTAL EEG | FDG PET | ICTAL SEMIOLOGY | SURGERY | SURGICAL OUTCOME |
|---------|-------------------------------------|---|-------------------------|--|--|------------------------------------|------------------|
| 1 | LT pole atrophy | LT slow wave activity and temporal spikes | LT ictal activity | left medial temporal hypoM + left anterior temporal neocortical hypoM | oro alimentary automatismes + right hand dystonia + loss of consciousness | left ATL | Ia (24 m) |
| 2 | LT post surgical sequelae | LT&RT spikes with left predominance | LT ictal activity | left medial temporal hypoM + right medial temporal hypoM | loss of consciousness + speech arrest | NA | NA |
| 3 | right HS | temporal spikes + temporal background slowing | RT basal ictal activity | right medial temporal + RT pole hypo M + RT lateral neocortical hypoM | left hand paresthesais + ascending visceral sensation + tachycardia + loss of consciousness post ictal confusion | right ATL | Ia (16 m) |
| 4 | left HS, LT pole atrophy | LT&RT spikes with left predominance | LT ictal activity | LT pole + LT lateral neocortical hypo M | oro alimentary automatismes + mental slowing with preserved consciousness | left ATL | Ia (48 m) |
| 5 | post surgical right temporal lesion | RT spikes | RT ictal activity | RT pole hypoM | loss of consciousness + bilateral dystonic arm posturing + oral automatismes | NA | NA |
| 6 | normal | normal | left central activity | left perisylvian hypo M including anterior temporal gyrus + temporal pole + insula | bilateral tonic posturing of arms + right head deviation + right arm paresthesias | left operculo insular thermolesion | Ia (4 m) |
| 7 | left amygdalar hyperintensity | LT spikes | LT ictal activity | LT pole hypoM + left medial temporal lobe hypoM | cephalic sensation + dreamy state + language disturbance | left medial temporal thermolesion | Ia (5 m) |
| 8 | right HS | RT slow wave activity | RT ictal activity | right medial temporal hypoM + right anterior temporal neocortical hypoM | oro alimentary automat. + preserved consciousness + left facial clonus | NA | NA |
| 9 | right HS | RT spikes | RT ictal activity | right medial temporal hypoM | verbal automatismes + dysgeusia + loss of consciousness | NA | NA |

Table 1. Clinical details of each patient. **legend;** HS: Hippocampal sclerosis / LT: left temporal / RT: right temporal / hypoM: hypometabolism / ATL: Anterior Temporal Lobectomy / NA: not performed / Surgical outcome is expressed as Engel Class

| | | SEIZURE ONSET | SEIZURE PROPAGATION | SEIZURE ENDING |
|--|-----------|---|---|--|
| Patient 1 | Seiz. 1 | Clinical: L ANT HIPPOC + L POST HIPPOC Method: subg3 + (subg1) | Clinical: L ANT HIPPOC + L POST HIPPOC + L TEMP POLE Method: subg3 + subg2 + (subg1) | Clinical: L ANT HIPPOC + L POST HIPPOC + L TEMP POLE + L ANT TEMP NEOCORTEX Method: subg4 + subg5 + subg6 + (subg1) |
| | Seiz. 2 | Clinical: L ANT HIPPOC + L POST HIPPOC Method: subg3 + (subg1) | Clinical: L ANT HIPPOC + L POST HIPPOC + L TEMP POLE Method: subg3 + subg2 + (subg1) | Clinical: L ANT HIPPOC + L POST HIPPOC + L TEMP POLE + L ANT TEMP NEOCORTEX Method: subg4 + subg5 + subg6 + (subg1) |
| | Seiz. 3 | Clinical: L ANT HIPPOC + L POST HIPPOC Method: subg3 + (subg1) | Clinical: L ANT HIPPOC + L POST HIPPOC + L TEMP POLE Method: subg3 + subg2 + (subg1) | Clinical: L ANT HIPPOC + L POST HIPPOC + L TEMP POLE + L ANT TEMP NEOCORTEX Method: subg4 + subg5 + subg6 + (subg1) |
| | subgraphs | subg1: L ANT HIPPOC + L AMYG, subg2: L ANT HIPPOC + L POST HIPPOC + L TEMPORAL POLE + L AMYG, subg3: L ANT HIPPOC + L POST HIPPOC + L POST TEMPORAL NEOCORTEX + L AMYG, subg4: L POST TEMPORAL NEOCORTEX + L TEMPORAL POLE + L ANT HIPPOC + L POST HIPPOC subg5: L ANT TEMPORAL NEOCORTEX + L TEMP POLE, subg6: L TEMPORAL POLE + L ANT TEMPORAL NEOCORTEX. | | |
| Patient 2 | Seiz. 1 | Clinical: L ANT HIPPOC + L POST HIPPOC Method: subg1 + (subg7) | Clinical: L ANT HIPPOC + L POST HIPPOC + L ANT TEMPORAL NEOCORTEX + L ORBITO FRONTAL NEOCORTEX Method: subg2 + (subg7) | Clinical: R ANT HIPPOC + R POST HIPPOC + R AMYG Method: subg3 + subg4 + subg5 + subg6 + (subg7) |
| | Seiz. 2 | Clinical: R ANT HIPPOC + R POST HIPPOC + R AMYG + R ENTORHINAL CORTEX Method: subg3 + subg4 + (subg7) | Clinical: R ANT HIPPOC + R POST HIPPOC + R AMYG + R ENTORHINAL CORTEX + R ANT TEMPORAL NEOCORTEX Method: subg5 + (subg7) | Clinical: L ANT HIPPOC + L POST HIPPOC Method: subg1 + subg2 + subg6 + (subg7) |
| | Seiz. 3 | Clinical: R ANT HIPPOC + R POST HIPPOC + R AMYG + R ENTORHINAL CORTEX Method: subg3 + subg4 + (subg7) | Clinical: R ANT HIPPOC + R POST HIPPOC + R AMYG + R ENTORHINAL CORTEX + R ANT TEMPORAL NEOCORTEX Method: subg5 + (subg7) | Clinical: L ANT HIPPOC + L POST HIPPOC Method: subg1 + subg5 + subg6 + (subg7) |
| | subgraphs | subg1: L ANT HIPPOC + L POST HIPPOC, subg2: L ANT HIPPOC + L POST HIPPOC + L ENTORHINAL CORTEX + L ORBITO FRONTAL CORTEX, subg3: R ANT HIPPOC + R POST HIPOC + R AMYG + R ENTORHINAL CORTEX, subg4: R ANT HIPPOC + R POST HIPOC + R AMYG + R ENTORHINAL CORTEX, subg5: R ANT HIPPOC + R POST HIPPOC + R ENTORHINAL CORTEX + R ORBITO FRONTAL CORTEX + R ANT TEMPORAL NEOCORTEX, subg6: R ANT TEMPORAL NEOCORTEX + R POST TEMPORAL NEOCORTEX, subg7: L ANT TEMPORAL NEOCORTEX | | |
| Legend; subg: subgraph, Seiz.: seizure, L: left, R: right, ANT HIPPOC: anterior hippocampus, POST HIPPOC: posterior hippocampus, ANT TEMPORAL NEOCORTEX: anterior temporal neocortex, POST TEMPORAL NEOCORTEX: posterior temporal neocortex, AMYG: amygdala. | | | | |

Table 2. Qualitative comparison between the set of activated structures determined by visual analysis and the BTND method for the patient 1 and 2

| | SEIZURE ONSET | SEIZURE PROPAGATION | SEIZURE ENDING |
|-----------|--|---|---|
| Patient 3 | Seiz. 1 Clinical: R ANT HIPPOC Method: (subg2) | Clinical: R ANT HIPPOC + R POST HIPPOC + R ENT CX Method: subg1 | Clinical: R ANT HIPPOC + R POST HIPPOC + R ENT CX + R TEMPORAL LATERAL + R OCCIPITAL CX + R PARIETAL CX + R POST CENTRAL OPERC Method: subg3 + subg4 + subg5 + subg6 |
| | Seiz. 2 Clinical: R ANT HIPPOC + R POST HIPPOC Method: (subg2) + subg3 + subg5 | Clinical: R ANT HIPPOC + R POST HIPPOC + R ENT CX Method: subg1 | Clinical: R ANT HIPPOC + R POST HIPPOC + R ENT CX + R TEMPORAL LATERAL + R OCCIPITAL CX + R PARIETAL CX + R POST CENTRAL OPERC Method: subg3 + subg4 + subg5 + subg6 |
| | Seiz. 3 Clinical: R ANT HIPPOC + R POST HIPPOC Method: (subg2) + subg3 + subg5 | Clinical: R ANT HIPPOC + R POST HIPPOC + R ENT CX + R TEMPORAL LATERAL + R OCCIPITAL CX + R PARIETAL CX + R POST CENTRAL OPERC Method: subg1 + (subg2) + subg4 + subg6 | Clinical: R ANT HIPPOC + R POST HIPPOC + R ENT CX + R TEMPORAL LATERAL + R OCCIPITAL CX + R PARIETAL CX + R POST CENTRAL OPERC Method: (subg2) + subg4 |
| subgraphs | subg1: R ANT HIPPOC + R POST HIPPOC + R AMYG + R ENT CX, subg2: R ANT HIPPOC, subg3: R PARIETAL CX + R OCCIPITAL CX, subg4: R TEMP LATERAL, subg5: R TEMP LATERAL + R POST CENTRAL OPERC, subg6: R TEMP LATERAL, | | |
| Patient 4 | Seiz. 1 Clinical: L ANT HIPPOC + L POST HIPPOC + L TEMP POLE Method: subg2 + (subg1) | Clinical: L ANT HIPPOC + L POST HIPPOC + L TEMP POLE + L POST TEMP NEOCORTEX + R AMYG + R ANT HIPPOC Method: subg3 + subg4 + subg5 | Clinical: L ANT HIPPOC + L POST HIPPOC + L TEMP POLE + L POST TEMP NEOCORTEX + R AMYG + R ANT HIPPOC Method: subg4 + subg5 + (subg6) |
| | Seiz. 2 Clinical: L ANT HIPPOC + L POST HIPPOC + L TEMP POLE Method: subg2 + (subg1) | Clinical: L ANT HIPPOC + L POST HIPPOC + L TEMP POLE + L POST TEMP NEOCORTEX + R AMYG + R ANT HIPPOC Method: subg3 + subg4 + subg5 | Clinical: L ANT HIPPOC + L POST HIPPOC + L TEMP POLE + L POST TEMP NEOCORTEX + R AMYG + R ANT HIPPOC Method: subg4 + subg5 + (subg6) |
| | Seiz. 3 Clinical: L ANT HIPPOC + L POST HIPPOC + L TEMP POLE Method: subg2 + (subg1) | Clinical: L ANT HIPPOC + L POST HIPPOC + L TEMP POLE + L POST TEMP NEOCORTEX + R AMYG + R ANT HIPPOC Method: subg3 + subg4 + subg5 | Clinical: L ANT HIPPOC + L POST HIPPOC + L TEMP POLE + L POST TEMP NEOCORTEX + R AMYG + R ANT HIPPOC Method: subg4 + subg5 + (subg6) |
| | Seiz. 4 Clinical: L ANT HIPPOC + L POST HIPPOC + L TEMP POLE Method: subg2 + (subg1) | Clinical: L ANT HIPPOC + L POST HIPPOC + L TEMP POLE + L POST TEMP NEOCORTEX + R AMYG + R ANT HIPPOC Method: subg3 + subg4 + subg5 | Clinical: L ANT HIPPOC + L POST HIPPOC + L TEMP POLE + L POST TEMP NEOCORTEX + R AMYG + R ANT HIPPOC Method: subg4 + subg5 + (subg6) |
| subgraphs | subg1: L ANT TEMP NEOCORTEX + R ANT HIPPOC, subg2: L ANT HIPPOC + L POST HIPPOC, subg3: L POST TEMPORAL NEOCORTEX + L AMYGDALA + L ANTERIOR CINGULATE, subg4: R AMYGD + R ANT HIPPOC + L ANT HIPPOC + L AMYG, subg5: R AMYGD + R ANT HIPPOC, subg6: L TEMP LATERAL + L TEMP POST | | |
| Patient 5 | Seiz. 1 Clinical: R ANT HIPPOC + R POST HIPPOC + R TEMP POLE + R AMYG Method: subg3 + (subg1) | Clinical: R ANT HIPPOC + R POST HIPPOC + R TEMP POLE + R AMYG Method: subg3 + subg2 + (subg1) | Clinical: R ANT HIPPOC + R POST HIPPOC + R TEMP POLE + R AMYG Method: subg3 + (subg4) + (subg1) |
| | Seiz. 2 Clinical: R ANT HIPPOC + R POST HIPPOC + R TEMP POLE + R AMYG Method: subg3 + (subg1) | Clinical: R ANT HIPPOC + R POST HIPPOC + R TEMP POLE + R AMYG + R POST TEMP NEOCORTEX Method: subg3 + subg2 + (subg1) | Clinical: R ANT HIPPOC + R POST HIPPOC + R TEMP POLE + R AMYG + R POST TEMP NEOCORTEX Method: subg3 + (subg4) + (subg1) |
| | Seiz. 3 Clinical: R ANT HIPPOC + R POST HIPPOC + R TEMP POLE + R AMYG Method: subg3 + (subg1) | Clinical: R ANT HIPPOC + R POST HIPPOC + R TEMP POLE + R AMYG + R POST TEMP NEOCORTEX + R ORBITO FRONTAL CX Method: subg3 + subg2 + (subg1) | Clinical: R ANT HIPPOC + R POST HIPPOC + R TEMP POLE + R AMYG + R POST TEMP NEOCORTEX R ORBITO FRONTAL CX Method: subg3 + (subg4) + (subg1) |
| | Seiz. 4 Clinical: R ANT HIPPOC + R POST HIPPOC + R TEMP POLE + R AMYG Method: subg3 + (subg1) | Clinical: R ANT HIPPOC + R POST HIPPOC + R TEMP POLE + R AMYG + R POST TEMP NEOCORTEX Method: subg3 + subg2 + (subg1) | Clinical: R ANT HIPPOC + R POST HIPPOC + R TEMP POLE + R AMYG + R POST TEMP NEOCORTEX Method: subg3 + (subg4) + (subg1) |
| subgraphs | subg1: R LAT TEMP NEOCORTEX + R LAT FRONTAL CORTEX, subg2: R ANT HIPPOC + R POST HIPPOC + R AMYG + R TEMPORAL POLE, subg3: R ANT HIPPOC + R POST HIPPOC + R POST HIPPOC + R ORBITO FRONTAL CX + R TEMPORAL POST NEOCORTEX | | |

Table 3. Qualitative comparison between the set of activated structures determined by visual analysis and the BTND method for the patient 3, 4 and 5. (see legend table 2)

| | SEIZURE ONSET | SEIZURE PROPAGATION | SEIZURE ENDING |
|-----------|---------------|---|--|
| Patient 6 | Seiz. 1 | Clinical: L PRECENTRAL OPERCULUM + L POST CENTRAL OPERCULUM + L FRONTAL CORTEX Method: subg2 + subg3 + subg4 + (subg1) (subg5) | Clinical: L PRECENTRAL OPERCULUM + L POST CENTRAL OPERCULUM + L FRONTAL CORTEX Method: subg4 + (subg1) (subg5) |
| | Seiz. 2 | Clinical: L PRECENTRAL OPERCULUM + L POST CENTRAL OPERCULUM + L FRONTAL CORTEX Method: subg2 + subg3 + subg4 + (subg1) (subg5) | Clinical: L PRECENTRAL OPERCULUM + L POST CENTRAL OPERCULUM + L FRONTAL CORTEX Method: subg4 + (subg1) (subg5) |
| | Seiz. 3 | Clinical: L PRECENTRAL OPERCULUM + L POST CENTRAL OPERCULUM + L FRONTAL CORTEX Method: subg2 + subg3 + subg4 + (subg1) (subg5) | Clinical: L PRECENTRAL OPERCULUM + L POST CENTRAL OPERCULUM + L FRONTAL CORTEX Method: subg4 + (subg1) (subg5) |
| | subgraphs | subg1: L PRECENTRAL OPERCULUM + L POST CENTRAL OPERCULUM + L FRONTAL CORTEX + L PARIETAL CORTEX subg3: L POST CENTRAL OPERCULUM + L PARIETAL CORTEX subg4: L TEMPORAL LOBE + L POST PARIETAL CORTEX | |
| Patient 7 | Seiz. 1 | Clinical: L ANT HIPPOC + L AMYGD + L POST HIPPOC + L AMYGD Method: subg2 + (subg1) | Clinical: L ANT HIPPOC + L POST HIPPOC + L AMYGD + L ANT TEMPORAL NEOCORTEX Method: subg3 (+subg1) |
| | subgraphs | subg1: L ANT TEMPORAL NEOCORTEX subg2: L ANT HIPPOC + L POST HIPPOC + L AMYGD subg3: L ANT HIPPOC + L POST HIPPOC + L AMYGD subg4: L ANT TEMPORAL NEOCORTEX subg5: L ANT TEMPORAL NEOCORTEX subg6: L ANT HIPPOC + L POST HIPPOC + L AMYGD | |
| Patient 8 | Seiz. 1 | Clinical: R ANT HIPPOC + R POST HIPPOC + R AMYG + R ENTORHINAL CORTEX + R TEMP POLE Method: subg3 + subg6 + (subg1) + (subg2) | Clinical: R ANT HIPPOC + R POST HIPPOC + R AMYG + R ENTORHINAL CORTEX + R TEMP POLE Method: subg1 + subg4 + subg5 + (subg2) |
| | Seiz. 2 | Clinical: R ANT HIPPOC + R POST HIPPOC + R AMYG + R ENTORHINAL CORTEX + R TEMP POLE Method: subg3 + subg6 + (subg2) | Clinical: R ANT HIPPOC + R POST HIPPOC + R AMYG + R ENTORHINAL CORTEX + R TEMP POLE Method: subg1 + subg4 + subg5 + (subg2) |
| | Seiz. 3 | Clinical: R ANT HIPPOC + R POST HIPPOC + R AMYG + R ENTORHINAL CORTEX + R TEMP POLE Method: subg3 + subg6 + (subg2) | Clinical: R ANT HIPPOC + R POST HIPPOC + R AMYG + R ENTORHINAL CORTEX + R TEMP POLE Method: subg3 + subg6 + (subg1) + (subg2) |
| | subgraphs | subg1: R ANT TEMPORAL NEOCORTEX + R POST TEMPORAL NEOCORTEX subg3: R ANT HIPPOC + R POST HIPPOC + R AMYG subg5: R ANT HIPPOC + R POST HIPPOC + R AMYG subg6: R ANT HIPPOC + R AMYG | |
| Patient 9 | Seiz. 1 | Clinical: R ANT HIPPOC + R POST HIPPOC + R AMYG + R ENTORHINAL CORTEX + R TEMP POLE Method: subg2 + (subg1) | Clinical: R ANT HIPPOC + R POST HIPPOC + R AMYG + R ENTORHINAL CORTEX + R TEMP POLE Method: subg3 + subg4 + subg5 + subg6 |
| | Seiz. 2 | Clinical: L ANT HIPPOC + L TEMP POLE Method: subg3 + (subg5) + (subg1) | Clinical: R ANT HIPPOC + R POST HIPPOC + R AMYG + R ENTORHINAL CORTEX + R TEMP POLE + L TEMP POLE Method: subg2 + subg3 + (subg5) + (subg1) |
| | Seiz. 2 | Clinical: L ANT HIPPOC + L TEMP POLE Method: subg3 + (subg5) + (subg1) | Clinical: R ANT HIPPOC + R POST HIPPOC + R AMYG + R ENTORHINAL CORTEX + R TEMP POLE + L TEMP POLE Method: subg2 + subg3 + (subg5) + (subg1) |
| | subgraphs | subg1: L POST TEMPORAL NEOCORTEX + L ANT TEMP NEOCORTEX + R ANT HIPPOC + R LAT TEMPORAL NEOCORTEX subg2: L ANT HIPPOC + L ANT TEMPORAL NEOCORTEX subg3: R ANT HIPPOC + R ENTORHINAL CX + R AMYG subg4: L ANT HIPPOC + L ANT TEMPORAL NEOCORTEX subg5: L POST TEMPORAL NEOCORTEX + L ANT TEMP NEOCORTEX + R ANT HIPPOC + R LAT TEMPORAL NEOCORTEX subg6: R ANT TEMPORAL NEOCORTEX + R POST TEMPORAL NEOCORTEX | |

Table 4. Qualitative comparison between the set of activated structures determined by visual analysis and the BTND method for the patient 6, 7, 8 and 9. (see legend table 2)